Target-directed microRNA degradation regulates developmental microRNA expression and embryonic growth in mammals

Benjamin T. Jones,[1] Jaeil Han,[1] He Zhang,[2] Robert E. Hammer,[3] Bret M. Evers,[4,5] Dinesh Rakheja,[4,6,7] Asha Acharya,[1,8] and Joshua T. Mendell[1,7,8,9]

[1]Department of Molecular Biology, University of Texas Southwestern Medical Center, Dallas, Texas 75390, USA; [2]Quantitative Biomedical Research Center, Peter O'Donnell Jr. School of Public Health, University of Texas Southwestern Medical Center, Dallas, Texas 75390, USA; [3]Department of Biochemistry, University of Texas Southwestern Medical Center, Dallas, Texas 75390, USA; [4]Department of Pathology, University of Texas Southwestern Medical Center, Dallas, Texas 75390, USA; [5]Department of Ophthalmology, University of Texas Southwestern Medical Center, Dallas, Texas 75390, USA; [6]Department of Pediatrics, University of Texas Southwestern Medical Center, Dallas, Texas 75390, USA; [7]Harold C. Simmons Comprehensive Cancer Center, University of Texas Southwestern Medical Center, Dallas, Texas 75390, USA; [8]Howard Hughes Medical Institute, University of Texas Southwestern Medical Center, Dallas, Texas 75390, USA; [9]Hamon Center for Regenerative Science and Medicine, University of Texas Southwestern Medical Center, Dallas, Texas 75390, USA

MicroRNAs (miRNAs) are post-transcriptional regulators of gene expression that play critical roles in development and disease. Target-directed miRNA degradation (TDMD), a pathway in which miRNAs that bind to specialized targets with extensive complementarity are rapidly decayed, has emerged as a potent mechanism of controlling miRNA levels. Nevertheless, the biological role and scope of miRNA regulation by TDMD in mammals remains poorly understood. To address these questions, we generated mice with constitutive or conditional deletion of *Zswim8*, which encodes an essential TDMD factor. Loss of *Zswim8* resulted in developmental defects in the heart and lungs, growth restriction, and perinatal lethality. Small RNA sequencing of embryonic tissues revealed widespread miRNA regulation by TDMD and greatly expanded the known catalog of miRNAs regulated by this pathway. These experiments also uncovered novel features of TDMD-regulated miRNAs, including their enrichment in cotranscribed clusters and examples in which TDMD underlies "arm switching," a phenomenon wherein the dominant strand of a miRNA precursor changes in different tissues or conditions. Importantly, deletion of two miRNAs, miR-322 and miR-503, rescued growth of *Zswim8*-null embryos, directly implicating the TDMD pathway as a regulator of mammalian body size. These data illuminate the broad landscape and developmental role of TDMD in mammals.

MicroRNAs (miRNAs) are ∼22-nt RNAs that negatively regulate messenger RNA (mRNA) stability and translation (Bartel 2018). miRNAs act as obligate cofactors for Argonaute (AGO) proteins, which they guide to target mRNAs primarily through base-pairing interactions between the miRNA 5′ end, termed the seed sequence, and complementary sites that are most often located in the 3′ untranslated regions (UTRs) of targets. Binding of AGO proteins results in recruitment of deadenylation and decapping complexes, leading to target repression (Jonas and Izaurralde 2015). Studies over the last two decades have established that miRNA-mediated regulation is critical for development and physiology in diverse metazoan species (Vidigal and Ventura 2015; Bartel 2018). Accordingly, elaborate mechanisms that impact miRNA abundance and activity have evolved to precisely control how miRNAs are deployed to regulate gene expression (Gebert and MacRae 2019).

Once loaded into an AGO protein, the 5′ and 3′ termini of the miRNA are deeply buried in the AGO middle (mid)

and PIWI/AGO/Zwille (PAZ) domains, respectively, thereby protecting the miRNA from exonucleolytic decay (Elkayam et al. 2012; Schirle and MacRae 2012). As a result, miRNAs are typically extremely stable, with half-lives extending to days or weeks in vivo (van Rooij et al. 2007; Gatfield et al. 2009; Kingston and Bartel 2019). Nevertheless, the existence of miRNAs with accelerated decay rates, first observed in mammalian cell lines (Hwang et al. 2007; Bail et al. 2010; Krol et al. 2010; Gantier et al. 2011; Rissland et al. 2011; Guo et al. 2015; Marzi et al. 2016; Kingston and Bartel 2019; Reichholf et al. 2019), foreshadowed the discovery of mechanisms that carry out sequence-specific miRNA degradation. Of the reported mechanisms of accelerated miRNA turnover, the most extensively studied is target-directed miRNA degradation (TDMD). TDMD is triggered when a miRNA engages specialized target sites with extended complementarity to both the seed sequence and the miRNA 3′ end. This miRNA decay pathway was initially discovered as a mechanism used by viruses to remodel host miRNA expression (Cazalla et al. 2010; Libri et al. 2012; Marcinowski et al. 2012; Lee et al. 2013) and simultaneously was shown to be induced by expression of highly complementary synthetic miRNA targets in *Drosophila* and human cells (Ameres et al. 2010). The subsequent identification of endogenous mammalian transcripts that function as triggers for TDMD (specifically *Cyrano*, *Nrep*, and *Serpine1*, which promote decay of miR-7, miR-29b, and miR-30b/c, respectively) established that this pathway is used as a natural mechanism to regulate the abundance of specific miRNAs in vivo (Bitetti et al. 2018; Ghini et al. 2018; Kleaveland et al. 2018).

Multiple studies recently reported the discovery of a cullin–RING ubiquitin ligase (CRL) complex containing the substrate adapter protein ZSWIM8 as a key mediator of TDMD (Han et al. 2020; Shi et al. 2020). The extensive complementarity between miRNAs and TDMD-inducing targets results in a conformational change in AGO (Sheu-Gruttadauria et al. 2019) that is believed to be specifically recognized by the ZSWIM8 complex. This results in AGO ubiquitylation, degradation by the proteasome, and consequent release of the miRNA for decay by cytoplasmic nucleases. When engaged with TDMD-inducing targets, the extended base pairing of the miRNA 3′ end also results in its release from the AGO PAZ domain (Sheu-Gruttadauria et al. 2019). This renders it susceptible to the activity of polymerases that add nontemplated nucleotides or exoribonucleases that remove nucleotides, a process termed tailing and trimming (Ameres et al. 2010). Although tailing and trimming are not essential for the activity of the ZSWIM8 complex or degradation of the miRNA (Han et al. 2020; Shi et al. 2020), their strong correlation with the TDMD pathway has proven to be a useful feature for identifying TDMD-inducing target transcripts (Li et al. 2021).

These advances in our understanding of the mechanism of TDMD have enabled broader investigation of the landscape of miRNAs that are regulated by this pathway in model organisms and cell lines. Indeed, loss of function of ZSWIM8 or its orthologs (EBAX-1 in *Caernorhabditis elegans* and Dora in *Drosophila*), coupled with small RNA sequencing, has revealed dozens of miRNAs that are strongly regulated by TDMD in mammalian cell lines (Han et al. 2020; Shi et al. 2020), *Drosophila* cell lines and embryos (Shi et al. 2020; Kingston et al. 2022), and adult *C. elegans* (Shi et al. 2020). For a subset of the newly identified mammalian and *Drosophila* TDMD-regulated miRNAs, decay-inducing target sites in both coding and noncoding transcripts that exhibit complementarity to both the miRNA seed sequence and 3′ end have been identified (Li et al. 2021; Kingston et al. 2022; Sheng et al. 2023). Interestingly, in *C. elegans*, miRNAs belonging to the *miR-35* family are degraded at the embryo to L1 transition in an EBAX-1-dependent manner, suggesting that they are additional substrates of the TDMD pathway (Donnelly et al. 2022). Nevertheless, degradation of these miRNAs relies only on their seed sequences, without a requirement for 3′ complementarity, suggesting the existence of alternative modes of recruiting ZSWIM8 orthologs for decay of specific miRNAs in worms and possibly other species.

The discovery of the ZSWIM8 complex has also allowed exploration of the biological roles of TDMD in animals. Dysregulation of miRNAs in Dora mutant *Drosophila* results in embryonic lethality and abnormal cuticle development, establishing an essential role for TDMD in development in flies (Kingston et al. 2022). Disentangling the developmental functions of ZSWIM8 homologs in *C. elegans* and mammals, however, has proven more challenging. Worms lacking EBAX-1 are viable and morphologically normal but exhibit an axon guidance defect that has been attributed to EBAX-1-mediated degradation of misfolded SAX-3, a receptor required for axonal pathfinding (Wang et al. 2013). Conditional deletion of *Zswim8* in mouse brains leads to incompletely penetrant perinatal lethality, reduced body size, and widespread neurodevelopmental abnormalities (Wang et al. 2023). These defects were reported to result, at least in part, from loss of ZSWIM8-mediated degradation of misfolded DAB1, a factor with pleiotropic functions in neuronal development. Thus, the role of TDMD in mammalian development and physiology, and the landscape of mammalian miRNAs regulated by this pathway in vivo, remain to be determined.

To address these outstanding questions, we generated mice harboring germline-transmitted and conditional *Zswim8* loss-of-function alleles. We observed several highly penetrant phenotypes in *Zswim8*$^{-/-}$ mice, including growth restriction in the developing embryo, defects in heart and lung development, and perinatal lethality. Small RNA sequencing of late embryonic tissues revealed widespread regulation of miRNAs by TDMD in vivo and greatly expanded the known set of miRNAs regulated by this pathway in mammals. Importantly, we demonstrated that stabilization of two cotranscribed miRNAs, miR-322 and miR-503, plays a causative role in growth restriction of *Zswim8*$^{-/-}$ embryos, thus establishing the TDMD pathway as a potent regulator of body size during mammalian development.

Results

Loss of ZSWIM8 causes perinatal lethality and developmental defects in mice

To investigate the biological role of TDMD in mammals, we used CRISPR/Cas9 genome editing of mouse zygotes to generate multiple constitutive and conditional *Zswim8* loss-of-function alleles. To achieve global loss of function, dual single-guide RNAs (sgRNAs) were used to delete *Zswim8* exons 2–7, which encode the BC-box and Cullin-2-box necessary for formation of the ZSWIM8 CRL complex (Wang et al. 2013), as well as the conserved SWIM domain (Fig. 1A). Loss of these exons is also predicted to result in a frameshift mutation that introduces a premature termination codon. Mice homozygous for this allele are referred to here as *Zswim8*$^{-/-}$. Additionally, we generated a conditional knockout allele by introducing loxP sites flanking exon 2 (Fig. 1A). Loss of this exon removes the BC-box and Cullin-2-box and disrupts the *Zswim8* reading frame. Animals homozygous for this allele are referred to as *Zswim8*$^{F/F}$.

Mice heterozygous for the exon 2–7 deletion were intercrossed to determine the consequences of global ZSWIM8 loss of function. Whereas wild-type and heterozygous animals were present at the expected frequencies at weaning (postnatal day 21 [P21]), no *Zswim8*$^{-/-}$ mice were observed at this time point (Fig. 1B). To determine at which stage *Zswim8*$^{-/-}$ mice were lost, timed matings were performed and litters were delivered by cesarean section at embryonic day 18.5 (E18.5). At this stage, all genotypes were observed at the expected Mendelian frequencies (Fig. 1B). We noted, however, that *Zswim8*$^{-/-}$ pups exhibited agonal breathing and died shortly after delivery. Furthermore, no *Zswim8*$^{-/-}$ mice survived to P1 (Fig. 1B). Thus, loss of *Zswim8* results in perinatal lethality in mice.

To determine the cause of perinatal death, we further examined *Zswim8*$^{-/-}$ embryos at E18.5. Western blotting confirmed the expected loss of ZSWIM8 protein in knockout tissues (Fig. 1C). *Zswim8*$^{-/-}$ embryos were significantly smaller than their wild-type and heterozygote littermates, with a >20% reduction in overall body weight (Fig. 2A,B). A complete necropsy of *Zswim8*$^{-/-}$ embryos further revealed overt and highly penetrant defects in heart morphology at this time point. Hearts from knockout animals were grossly smaller and globose in shape, lacking a distinct apex (Fig. 2C). Histologic analysis revealed dilated ventricular cavities with thinning and non-compaction of ventricular walls (Fig. 2D). We additionally observed ventricular septal defects (VSDs) in approximately one-third of *Zswim8*$^{-/-}$ hearts (Supplemental Fig. S1A).

To determine whether abnormal cardiac development was the cause of perinatal lethality, we crossed mice carrying the floxed *Zswim8* allele to mice harboring a *Nkx2.5*-Cre transgene that is expressed as early as E7.5 in the cardiac crescent and in the majority of heart tube progenitor cells (McFadden et al. 2005). Although we observed a slight undertransmission of the *Nkx2.5*-Cre transgene overall, *Nkx2.5*-Cre; Z*swim8*$^{+/+}$ and *Nkx2.5*-Cre; Z*swim8*$^{F/F}$ mice were equally represented at P21 (Supplemental Fig. S1B). Moreover, the body weights of *Nkx2.5*-Cre; Z*swim8*$^{F/F}$ mice at E18.5 were equivalent to control animals (Supplemental Fig. S1C). Notably, *Nkx2.5*-Cre; Z*swim8*$^{F/F}$ mice exhibited developmental
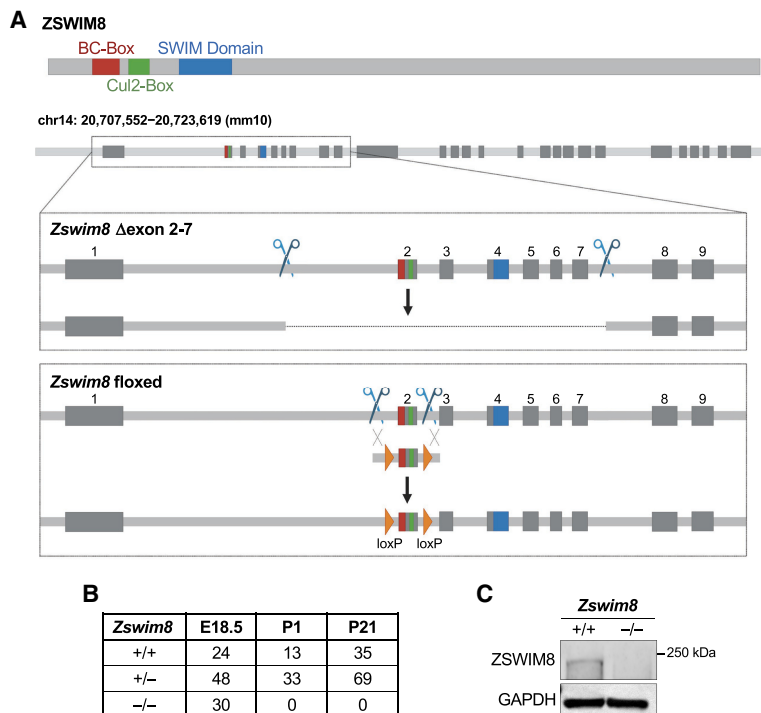

Figure 1. Loss of ZSWIM8 results in perinatal lethality in mice. (*A*) Genome-editing strategy used to generate *Zswim8*$^{-/-}$ (Δexon 2–7) and *Zswim8*$^{F/F}$ (floxed) mice. (*Top*) Schematic of ZSWIM8 protein with approximate locations of the BC-box (red), Cul2-box (green), and SWIM domain (blue) indicated. (*Bottom*) Depiction of the mouse *Zswim8* genomic locus with exons encoding each domain in the appropriate color as defined in *top* panel, scissors showing CRISPR–Cas9 targeting sites, and a DNA segment with orange triangles indicating donor sequence-containing loxP sites. (*B*) Frequency of genotypes of offspring produced from *Zswim8*$^{+/-}$ intercrosses at the indicated time points. (*C*) Western blot of ZSWIM8 protein in E18.5 brains from embryos of the indicated genotypes.

Zswim8	E18.5	P1	P21
+/+	24	13	35
+/–	48	33	69
–/–	30	0	0

heart defects that resembled those observed in $Zswim8^{-/-}$ embryos, including less defined apices and dilation of the ventricles, though these phenotypes were less severe than those observed in global knockout animals (Supplemental Fig. S1D). Quantitative PCR documented successful recombination of the floxed allele in $Nkx2.5$-Cre; $Zswim8^{F/F}$ hearts (Supplemental Fig. S1E). Although a significant fraction of detectable alleles remained unrecombined, this was likely due in part to a contribution from noncardiac lineages. Overall, these data demonstrated that intrinsic deficiency of ZSWIM8 in the embryonic heart impairs cardiac development, but these abnormalities may not account for perinatal lethality of $Zswim8^{-/-}$ mice. It remains possible, however, that earlier and/or complete loss of the protein in developing hearts of germline $Zswim8$ knockout animals produces more severe cardiac defects that are incompatible with postnatal viability.

Seeking other potential causes of neonatal death of $Zswim8^{-/-}$ mice, we next examined the lungs of these an-imals. Defects in lung development are a common cause of perinatal lethality (Turgeon and Meloche 2009) and were of particular interest due to the agonal breathing displayed by newborn $Zswim8^{-/-}$ mice. At E16.5, mouse lungs enter the canalicular stage of development, in which the respiratory tree expands and is vascularized (Warburton et al. 2010). This is followed by the saccular stage, extending from E17.5 to P5, during which thinning of the septa occurs, alveolar airspaces expand, and epithelial cells differentiate into the alveolar type I and type II pneumocytes to produce surfactant. Lungs were harvested from E18.5 $Zswim8^{+/+}$ and $Zswim8^{-/-}$ mice before animals initiated breathing. As expected, wild-type lungs displayed features characteristic of the mid to late saccular stage of development, with emerging airspaces and thinning alveolar septa (Fig. 2E,F). Lungs from $Zswim8^{-/-}$ embryos, in contrast, appeared less mature, with less expanded saccules, thicker septa, and minimally expanded terminal airspaces. These findings were indicative of the late canalicular stage of development. Thus, ZSWIM8
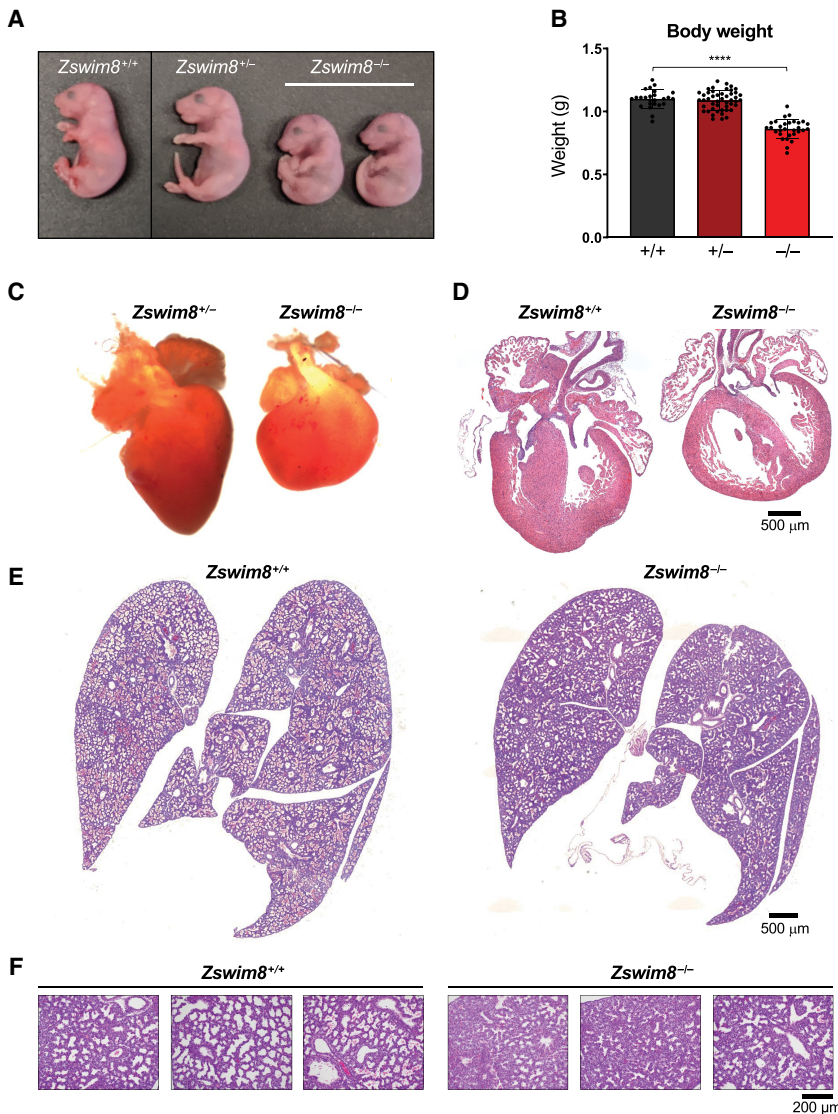

Figure 2. ZSWIM8 deficiency leads to growth restriction and defective heart and lung development. (A) Images of E18.5 mice of the indicated genotypes. (B) Body weights of E18.5 mice of the indicated genotypes. $n=25$ $Zswim8^{+/+}$, $n=47$ $Zswim8^{+/-}$, $n=30$ $Zswim8^{-/-}$. Data are represented as mean ± SD, with individual data points shown. (****) $P<0.0001$ (unpaired t-test). (C) Images of E18.5 hearts of the indicated genotypes. (D–F) Representative hematoxylin and eosin (H&E)-stained sections of E18.5 hearts (D) and lungs (E,F) of the indicated genotypes.

deficiency resulted in delayed lung development, providing a likely explanation for respiratory failure in newborn Zswim8$^{-/-}$ mice. Altogether, these results established an essential role for ZSWIM8 in mammalian development, with critical roles in organogenesis of the heart and lungs and in regulation of body size.

The landscape of TDMD-regulated miRNAs in mammalian tissues

We hypothesized that the stabilization of miRNAs that are normally degraded through the TDMD pathway contributes to the developmental defects observed in Zswim8$^{-/-}$ mice. To identify such miRNAs and to comprehensively characterize the landscape of mammalian miRNAs that are regulated by TDMD in vivo, we performed small RNA sequencing on a broad panel of tissues from E18.5 Zswim8$^{+/+}$ and Zswim8$^{-/-}$ mice (brain, heart, lung, liver, small intestine, kidney, skin, and stomach). These studies revealed numerous miRNAs that were strongly up-regulated in Zswim8$^{-/-}$ tissues (Fig. 3A; Supplemental Table S1). To distinguish between miRNAs that were up-regulated due to increased transcription or processing, possibly as a secondary consequence of the developmental abnormalities in ZSWIM8-deficient tissues, and those whose stability was increased due to abrogation of TDMD, we examined both strands of each miRNA duplex. TDMD occurs after the loading of the mature miRNA into AGO (Han et al. 2020; Shi et al. 2020), which separates it from the opposite strand of the processed miRNA duplex, also known as the passenger strand or miRNA*. As a consequence, direct TDMD substrates are expected to be up-regulated upon loss of ZSWIM8 without an increase in abundance of the opposite strand. On the basis of this criterion, we detected 57 miRNAs that behaved as direct substrates of the TDMD pathway in at least one tissue, thereby nearly doubling the known number of miRNAs regulated by TDMD in mammals (Fig. 3B). While many miRNAs were broadly controlled by TDMD across all sequenced tissues, some were regulated in a tissue-specific manner, suggesting the restricted expression of the target transcripts that induce their decay. Northern blotting of a selected panel of miRNAs confirmed their robust up-regulation in ZSWIM8-deficient tissues (Fig. 3C; Supplemental Fig. S2).

During the loading of miRNAs into AGO, the strands of the processed miRNA duplex are discriminated such that loading of the mature miRNA, or guide strand, is favored, while the dissociated passenger strand is discarded and degraded (Kim et al. 2009). Consequently, the more abundant strand is generally defined as the guide, and the less abundant strand is designated the passenger, although examples in which both strands are loaded and regulate targets have been described (Medley et al. 2021). We observed that 12 of the 57 ZSWIM8-regulated miRNAs represented the normally less abundant strand of the miRNA duplex (miR-99a-3p, miR-99b-3p, miR-149-3p, miR-154-3p, miR-335-3p, miR-379-3p, miR-411-3p, miR-429-5p, miR-652-5p, miR-702-5p, miR-3102-5p, and miR-3544-5p), suggesting that these miRNAs are loaded into AGO

and actively engage targets despite being annotated as passenger strands. For four of these miRNAs (miR-154, miR-335, miR-411, and miR-3544), the normally less abundant strand became the more abundant strand in one or more ZSWIM8-deficient tissues (Fig. 4A). The phenomenon in which the dominant strand of a miRNA duplex changes in different cell types or conditions has been referred to as "arm switching" and is generally believed to be a mechanism for regulating miRNA activity that operates at the AGO loading step (Grimson et al. 2008; Marco et al. 2010; Cloonan et al. 2011; Griffiths-Jones et al. 2011; Li et al. 2011, 2012). Our data suggested that some examples of arm switching may be a consequence of differential regulation of specific miRNA strands by the TDMD pathway. For example, miR-154, a miRNA that has been reported to undergo arm switching (Cheng et al. 2013), exhibits 3′ (3p) dominance in the brain, intestine, liver, and lungs while exhibiting 5p dominance in the heart, kidneys, skin, and stomach (Fig. 4A). In Zswim8$^{-/-}$ mice, however, all tissues exhibit a strong miR-154-3p bias, suggesting that differential regulation of the 3p strand by TDMD across tissues most likely accounts for the apparent arm switching of this miRNA.

Another interesting feature of mammalian TDMD substrates is their organization in clusters. While ~25% of all miRNAs are encoded in clusters (Kabekkodu et al. 2018), we observed that 36 out of 57 TDMD-regulated miRNAs (63%) were organized in this manner. This enrichment for clustered miRNAs is more than expected by chance ($P < 0.0001$, χ^2 test). In total, we detected members of 14 different miRNA clusters that were regulated by TDMD, notably including miRNAs encoded in a very large imprinted cluster on mouse chromosome 12 and members of the oncogenic miR-17-92 and paralogous clusters, among others (Fig. 4B; Supplemental Fig. S3). In some cases, individual cluster members were regulated by TDMD across all examined tissues, such as miRNAs derived from the imprinted chromosome 12 cluster and the miR-322-450b cluster (Fig. 4B). In other instances, clustered miRNAs were only regulated by TDMD in specific tissues, as exemplified by members of the miR-466 cluster (Supplemental Fig. S3). Considering that clustered miRNAs are generally cotranscribed, these results demonstrate that the TDMD pathway is used as a means to post-transcriptionally regulate the expression of individual miRNAs within clusters in a tissue-specific manner.

Tailing and trimming of TDMD-regulated miRNAs

It has been shown that extensive complementarity between the 3′ region of a miRNA and a TDMD-inducing target can stimulate the addition or removal of nucleotides from the miRNA 3′ end, a process known as tailing and trimming (Ameres et al. 2010). Although tailing and trimming are not required for TDMD (Han et al. 2020; Shi et al. 2020), their association with this pathway has been used as a feature to identify target transcripts that promote TDMD (Li et al. 2021). Moreover, in cell lines, loss of ZSWIM8 can increase the abundance of tailed and trimmed miRNAs that are normally regulated by TDMD (Han et al.
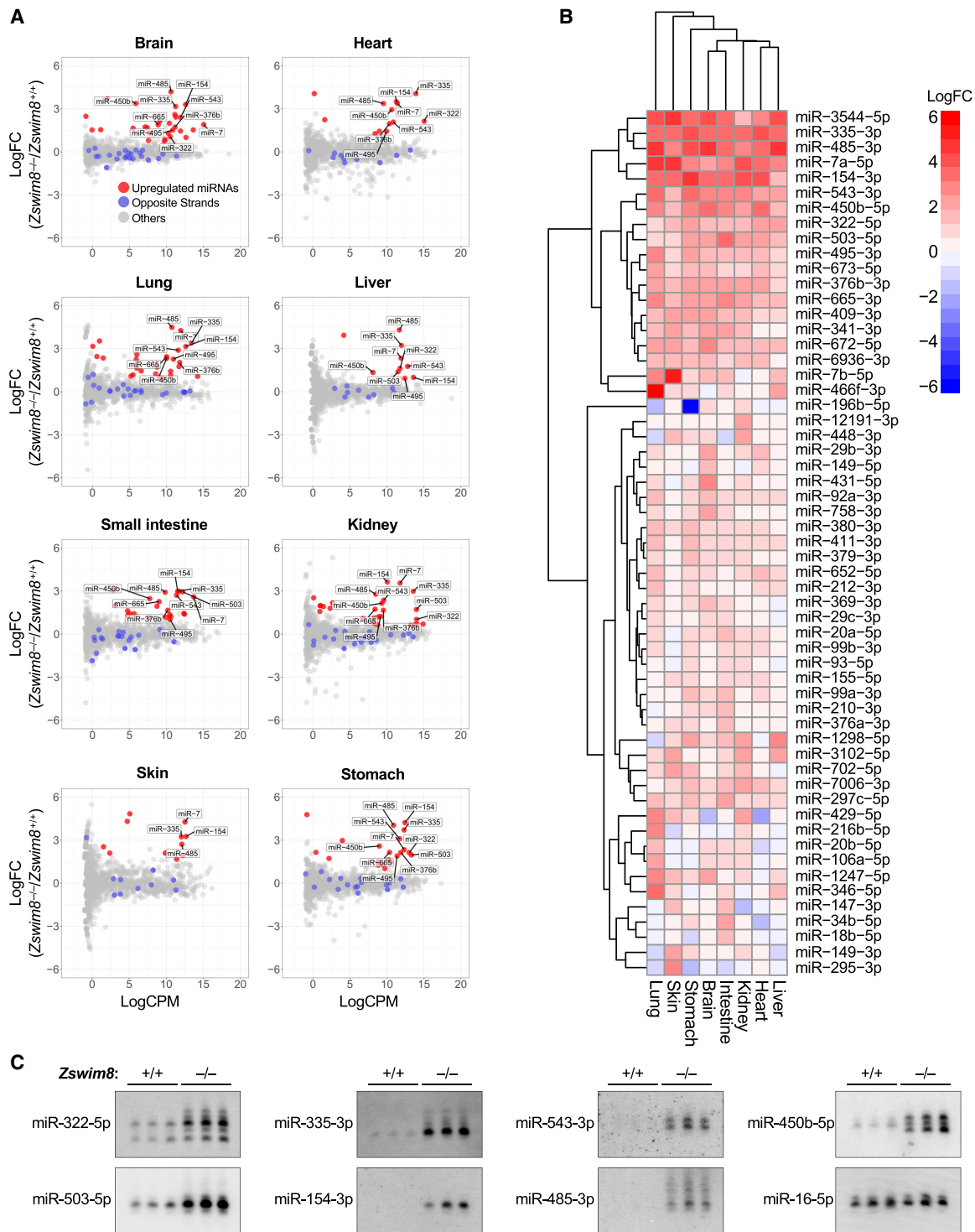
Figure 3. The landscape of TDMD-regulated miRNAs in mouse embryonic tissues. (*A*) Small RNA sequencing of E18.5 tissues. Red dots show miRNAs that were significantly up-regulated in $Zswim8^{-/-}$ relative to $Zswim8^{+/+}$ tissues ($P < 0.05$; FDR < 0.05) without a corresponding increase in the opposite strand derived from the same precursor (labeled with blue dots). $n = 3$ biological replicates per genotype. (LogFC) Log$_2$ fold change, (LogCPM) log$_2$ counts per million in $Zswim8^{+/+}$ tissue. (*B*) Heat map showing log$_2$ fold change of all TDMD-regulated miRNAs ($Zswim8^{-/-}/Zswim8^{+/+}$), defined as those exhibiting significant up-regulation in at least one $Zswim8^{-/-}$ tissue ($P < 0.05$; FDR < 0.05) without a corresponding increase in the opposite strand derived from the same precursor. (*C*) Northern blot analysis of miRNA expression in E18.5 hearts from mice of the indicated genotypes. $n = 3$ biological replicates per genotype. miR-16-5p served as a loading control.

2020; Shi et al. 2020), presumably by stabilizing the interaction between miRNAs and TDMD-inducing targets that leads to modification of the miRNA 3′ end. Our Northern blot analyses confirmed that a subset of TDMD-regulated miRNAs in mouse tissues undergoes tailing and trimming (Fig. 3C; Supplemental Fig. S2). To examine this phenomenon more globally, the proportion of tailed or trimmed miRNA species in small RNA sequencing data from $Zswim8^{+/+}$ and $Zswim8^{-/-}$ mice was assessed. We observed a wide range of tailing and trimming of TDMD substrates in all tissues, with some miRNAs exhibiting negligible 3′ modification (Supplemental Fig. S4A,B; Supplemental Table S2). In most tissues, the overall magnitude of tailing or trimming of TDMD substrates was not higher than the tailing or trimming of all other miRNAs, consistent with the existence of TDMD-independent pathways that modify miRNA 3′ ends (Shukla et al. 2019; Jeong et al. 2023). Nevertheless, the increase in tailing and trimming of individual miRNAs observed upon loss of ZSWIM8 was greater for TDMD substrates compared with non-TDMD-regulated miRNAs in nearly all tissues (Fig. 5A,B). In half of the examined tissues, the magnitude of regulation of a miRNA by TDMD was positively correlated with its increased tailing and/or trimming upon loss of ZSWIM8 (Fig. 5C; Supplemental Fig. S4C). Overall, these data confirmed that while many miRNAs undergo tailing and trimming in vivo, the abundance of tailed and trimmed isoforms of TDMD-regulated miRNAs is more sensitive to depletion of ZSWIM8 compared with miRNAs that are not regulated by this pathway. The fact that a subset of TDMD-regulated miRNAs do not undergo tailing and trimming may indicate that some miRNAs engage in alternative base-pairing configurations with their cognate TDMD-inducing triggers that do not expose the miRNA 3′ end.

Growth restriction of $Zswim8^{-/-}$ mice is attributable to up-regulation of miR-322 and miR-503

Among the most abundant miRNAs that were regulated by TDMD across multiple tissues were miR-322 and miR-503 (Fig. 3A,B), which are cotranscribed as part of a larger cluster of miRNAs located on the X chromosome (Fig. 4B). These miRNAs have previously been identified as TDMD substrates in murine cell lines (Rissland et al. 2011; Shi et al. 2020). As members of the miR-15/16 family, a highly studied group of miRNAs that regulate the cell cycle and apoptosis (Aqeilan et al. 2010), we wondered whether dysregulation of miR-322 and miR-503 contributed to the developmental abnormalities observed in $Zswim8^{-/-}$ mice. To investigate this possibility, Cas9 and dual sgRNAs were used to generate mice harboring a genomic deletion encompassing these miRNAs (Fig. 6A). As reported previously (Llobet-Navas et al. 2014), loss of these miRNAs had no effect on embryonic viability, and mice carrying the knockout allele were present at Mendelian ratios at weaning (Supplemental Fig. S5A,B). Northern blotting confirmed the complete loss of expression of miR-322 and miR-503 in knockout tissues (Fig. 6B).

Mice carrying null alleles of $miR-322/503$ and $Zswim8$ were then intercrossed to generate double-knockout animals. As observed in $Zswim8$ single-knockout mice, female $Zswim8^{-/-}$; $miR-322/503^{-/-}$ and male $Zswim8^{-/-}$; $miR-322/503^{-/Y}$ mice died shortly after birth and were not present at weaning (Supplemental Fig. S5A,B). In line with the observed perinatal lethality of these animals, E18.5 double-knockout mice exhibited malformed, globose hearts with poorly defined apices and VSDs, as well as immature lungs at the late canalicular stage (Fig. 6C–E; Supplemental Fig. S5C). In contrast to these similarities between $Zswim8$ single-knockout mice and $Zswim8$; $miR-322/503$ double knockouts, we observed that loss of miR-322 and miR-503 was sufficient to rescue embryonic growth of ZSWIM8-deficient mice (Fig. 6F–H). Analysis of body weights of E18.5 female mice enabled determination of the contribution of individual $miR-322/503$ alleles to embryonic body size. Haploinsufficiency of $miR-322/503$ resulted in significantly larger $Zswim8^{-/-}$ embryos but did not significantly impact body weight in $Zswim8^{+/+}$ mice (Fig. 6G). Homozygous loss of these miRNAs led to a full normalization of body size in the $Zswim8^{-/-}$ background while also significantly increasing the growth of wild-type embryos. In males, where only complete absence of miR-322 and miR-503 could be examined since these miRNAs are encoded on the X chromosome, we again observed that deletion of $miR-322/503$ increased body size in $Zswim8^{+/+}$ animals but had a stronger effect in $Zswim8^{-/-}$ mice, fully rescuing body size in this setting (Fig. 6H). Together, these results demonstrated that the $miR-322/503$ locus is a dose-dependent negative regulator of embryonic growth and revealed that up-regulation of the encoded miRNAs contributed to the small body size phenotype of $Zswim8^{-/-}$ mice. These data therefore established the TDMD pathway as a regulator of embryonic growth in mammals.

Discussion

TDMD was initially discovered as a mechanism of miRNA decay that can be induced by exogenously introduced targets, including transcripts encoded by viruses and synthetic targets with extensive miRNA complementarity (Ameres et al. 2010; Cazalla et al. 2010). The subsequent identification of a select group of endogenous miRNA:target pairs that trigger TDMD demonstrated that this pathway is a physiologic mechanism used to control miRNA abundance, though the number of known TDMD substrates remained limited (Bitetti et al. 2018; Ghini et al. 2018; Kleaveland et al. 2018; Li et al. 2021). The recent discovery of the ZSWIM8 ubiquitin ligase, which is essential for miRNA decay by TDMD (Han et al. 2020; Shi et al. 2020), has now enabled the direct experimental analysis of the scope and biological role of this pathway in diverse metazoan species (Kingston et al. 2022). Here we report the phenotypic consequences of ZSWIM8 loss of function in mice and characterize the landscape of TDMD-regulated miRNAs in mammalian tissues. These studies revealed that the TDMD pathway is required for normal mammalian development and is essential for establishing the appropriate expression of a broad set of miRNAs in vivo.
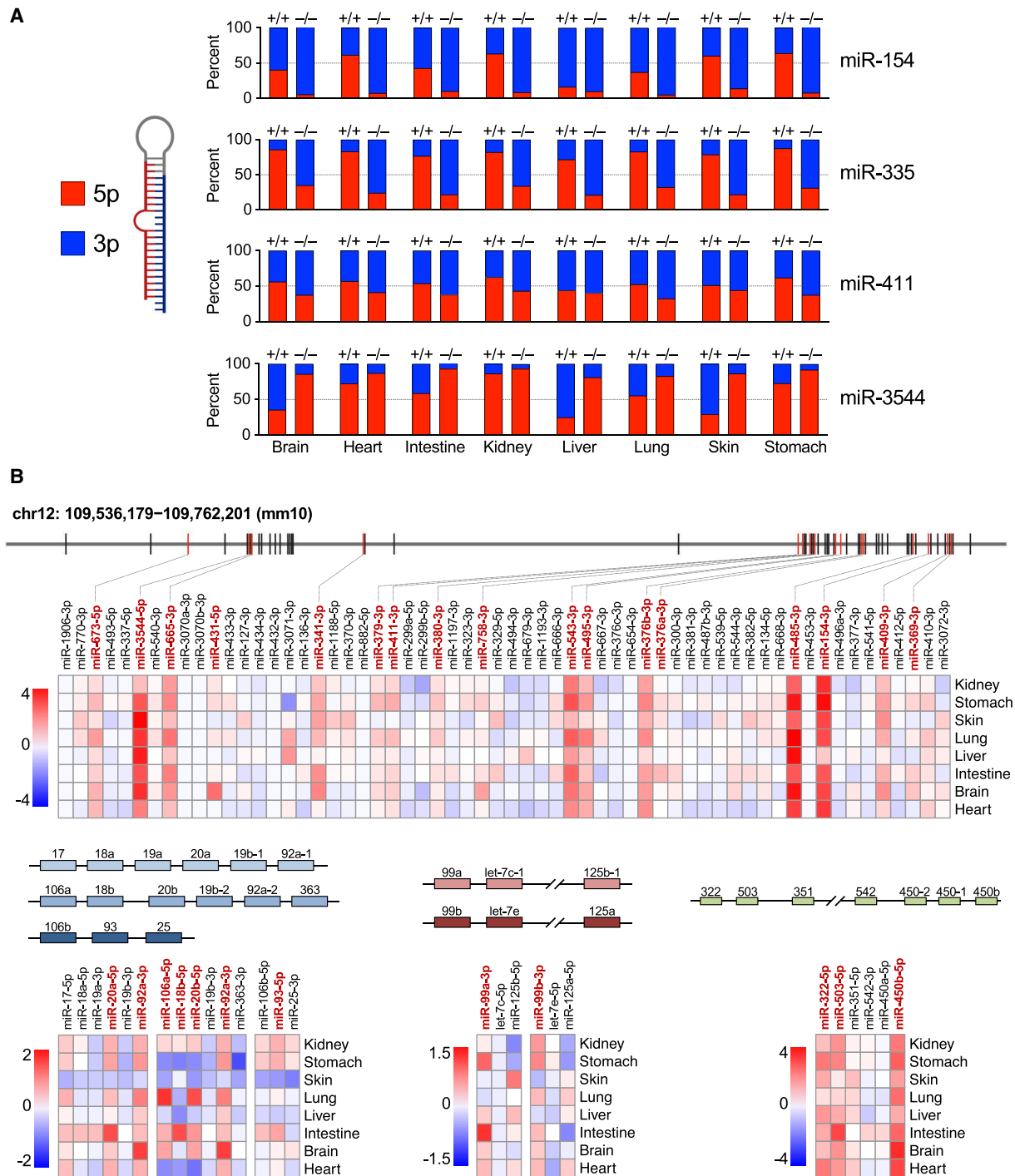
Figure 4. TDMD regulates nondominant miRNA strands, arm switching, and clustered miRNAs. (*A*) Stacked bar graphs showing the relative abundance of 5p and 3p strands of the indicated miRNAs in E18.5 tissues from $Zswim8^{+/+}$ or $Zswim8^{-/-}$ mice. (*B*) Schematic representation of miRNA clusters encoding TDMD-regulated miRNAs. Heat maps display $\log_2$ fold change of miRNA expression ($Zswim8^{-/-}/Zswim8^{+/+}$) for each cluster member across tissues. miRNAs labeled in red text are TDMD substrates in at least one tissue.

Global loss of ZSWIM8 resulted in an array of developmental defects in mice, including malformed hearts, immature lungs, and embryonic growth restriction, ultimately leading to fully penetrant perinatal lethality.

Cardiac-specific loss of ZSWIM8 partially recapitulated the observed defects in heart development but did not result in perinatal death. While the survival of heart-specific *Zswim8* knockout mice could be due to depletion of
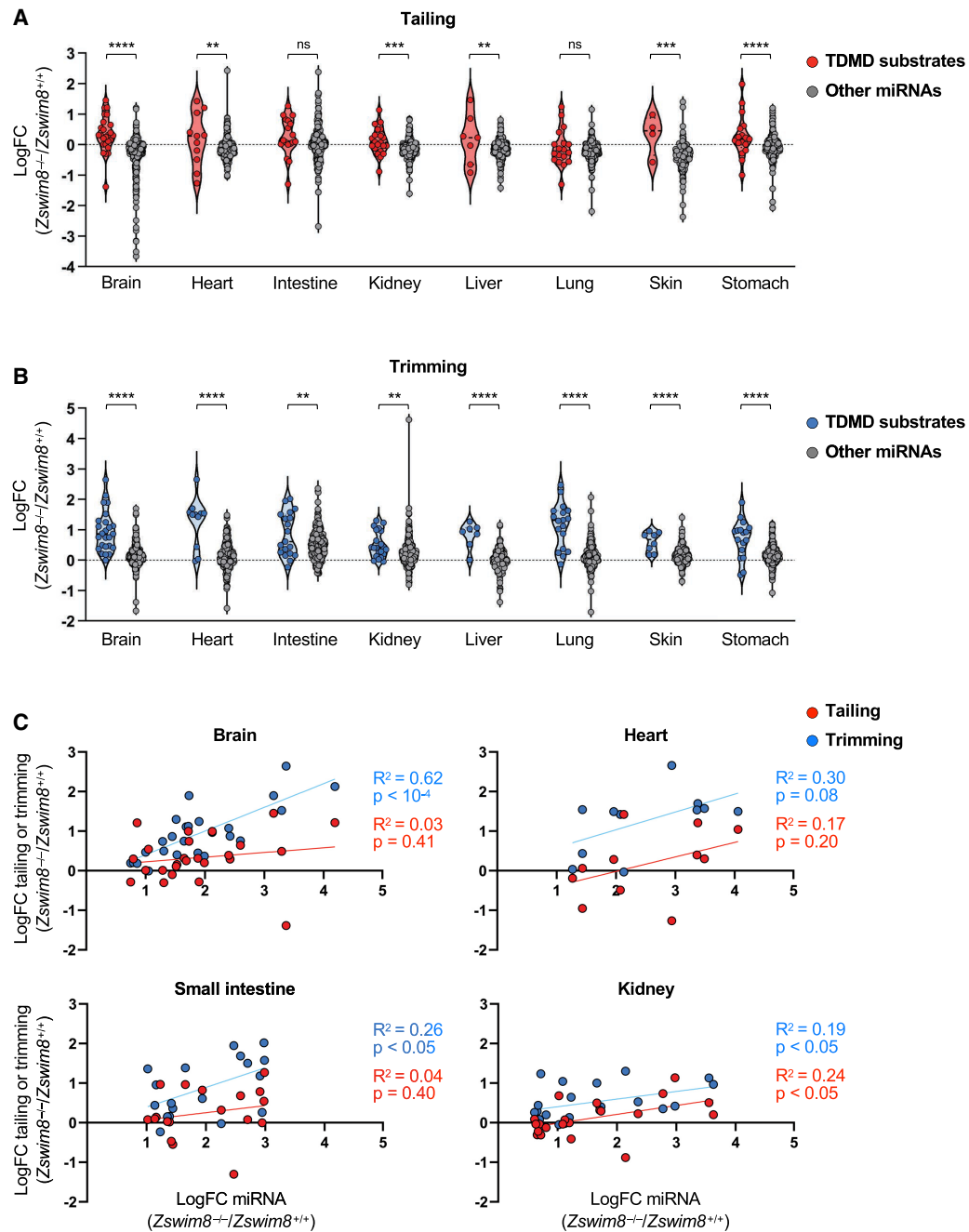
Figure 5. Tailing and trimming of TDMD-regulated miRNAs in mouse tissues. (A,B) Violin plots showing the $\log_2$ fold change ($Zswim8^{-/-}/Zswim8^{+/+}$) of tailing (A) or trimming (B) of miRNAs in E18.5 tissues. (ns) Not significant, (****) $P < 0.0001$, (***) $P < 0.001$, (**) $P < 0.01$ (unpaired t-test). (C) Scatter plots showing the $\log_2$ fold change of tailing or trimming of each TDMD-regulated miRNA relative to its $\log_2$ fold change in abundance ($Zswim8^{-/-}/Zswim8^{+/+}$) in each tissue.

ZSWIM8 at a later developmental time point compared with germline knockout animals, we speculate that delayed development of $Zswim8^{-/-}$ lungs likely contributed to postnatal inviability, given that newborn animals exhibited clear signs of respiratory distress. Future studies using lung-specific Cre driver lines are warranted to further investigate the role of ZSWIM8 in the developing lungs.

The survival of $Zswim8^{-/-}$ mice to birth enabled a comprehensive analysis of the repertoire of TDMD-regulated miRNAs in a broad set of late embryonic tissues. These studies revealed several notable features of the mammalian TDMD pathway. First, we detected 57 miRNAs that behaved as TDMD substrates in at least one tissue, as defined by a statistically significant increase in the abundance of the miRNA in $Zswim8^{-/-}$ mice without an
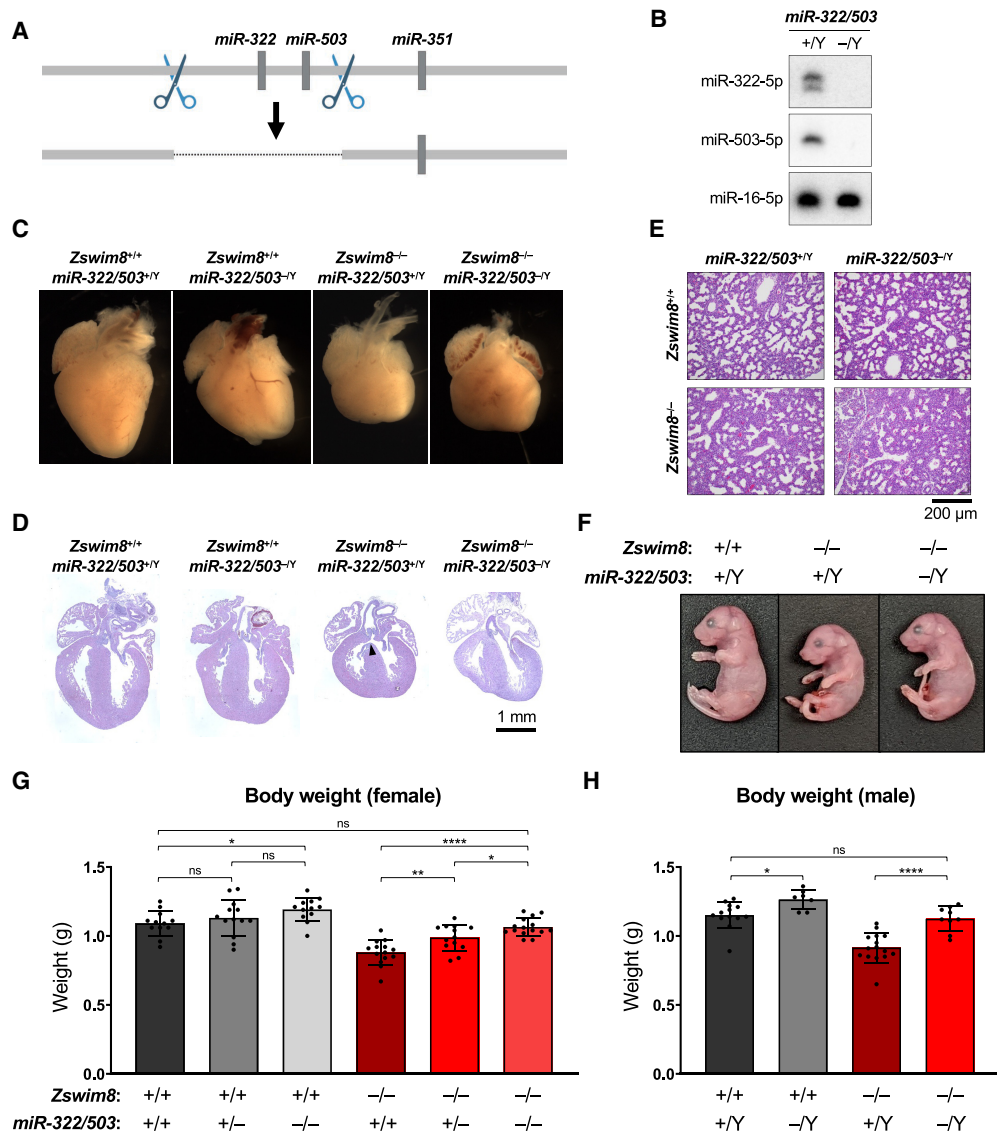
Figure 6. Loss of miR-322 and miR-503 rescues embryonic growth in $Zswim8^{-/-}$ mice. (*A*) Genome-editing strategy used to generate $miR-322/503^{-/-}$ mice. Scissors depict the approximate location of CRISPR–Cas9 targeting sites. (*B*) Northern blot analysis of miRNA expression in E18.5 hearts of the indicated genotypes. (*C*) Images of E18.5 hearts of the indicated genotypes. (*D,E*) H&E-stained sections of E18.5 hearts (*D*) and lungs (*E*) of the indicated genotypes. VSD in a $Zswim8^{-/-}$; $miR-322/503^{+/Y}$ heart, indicated with an arrowhead in *D*. (*F*) Images of E18.5 mice of the indicated genotypes. (*G,H*) Body weights of E18.5 female (*G*) and male (*H*) mice of the indicated genotypes. $n = 7–15$ mice per genotype. Data are represented as mean ± SD, with individual data points shown. (ns) Not significant, (****) $P < 0.0001$, (**) $P < 0.01$, (*) $P < 0.05$ (unpaired *t*-test).

increase in the opposite strand derived from the same precursor. Prior to this study, two mammalian miRNAs were identified as TDMD substrates in mouse tissues (Bitetti et al. 2018; Kleaveland et al. 2018), and another 32 miRNAs were shown to be regulated by this pathway in mammalian cell lines (Ghini et al. 2018; Han et al. 2020; Shi et al. 2020; Li et al. 2021). Our results therefore considerably expand the known catalog of TDMD-regulated miRNAs and suggest that this miRNA turnover pathway may be more active in vivo compared with cell lines. We speculate that this increased repertoire of TDMD substrates may reflect a need to efficiently clear specific miRNAs

during rapidly timed developmental transitions that are not modeled in cultured cells where mammalian TDMD has been previously studied. Additionally, it may be advantageous to regulate miRNAs via TDMD in terminally differentiated, nondividing cells in somatic tissues since, in contrast to cell lines, miRNAs cannot be diluted by cell division upon transcriptional shutoff in this setting. A second major feature of TDMD-regulated miRNAs in mammals is their frequent organization in genomic clusters. Thirty-six out of the 57 TDMD-regulated miRNAs are derived from clusters, representing significant enrichment. Since clustered miRNAs are generally

cotranscribed, TDMD appears to be regularly used as a mechanism to uncouple the expression of individual cluster members. Third, we identified examples of miRNAs in which the nondominant strand was strongly regulated by TDMD and, in some cases, became the dominant strand in specific ZSWIM8-deficient tissues. This observation suggests that some examples of the previously described phenomenon of "arm switching," in which the dominant miRNA strand from a miRNA precursor varies across cell types or conditions, may be due to selective decay of one miRNA strand by the TDMD pathway. Indeed, we found that tissue-specific differences in the magnitude of downregulation of the 3p strand of miR-154 by TDMD provides a mechanistic explanation for the reported arm switching of this miRNA across tissues (Cheng et al. 2013). Altogether, these data illuminate the broad scope of TDMD in mammalian tissues and reveal previously unrecognized roles for this pathway in shaping miRNA expression in vivo.

The phenotypic consequences of ZSWIM8 loss of function vary across metazoan species. In *C. elegans*, loss of the ZSWIM8 ortholog EBAX-1 results in neuromuscular defects, reduced egg laying, and decreased male mating (Wang et al. 2013). Deficiency of Dora, the ZSWIM8 ortholog in *Drosophila*, leads to embryonic lethality and defective cuticle development (Kingston et al. 2022). As reported here, mouse ZSWIM8 is essential for normal heart and lung development, embryonic growth, and postnatal viability. However, as a component of a ubiquitin ligase complex, ZSWIM8 may regulate the stability of multiple proteins in addition to AGO, thus complicating the interpretation of these phenotypes. Indeed, ZSWIM8 homologs in *C. elegans* and mice have been reported to impact neurodevelopmental phenotypes by controlling the stability of proteins involved in axon guidance and brain development (Wang et al. 2013, 2023). Thus far, the strongest evidence that the TDMD pathway itself plays an important role in regulating miRNA expression during development comes from studies of *Drosophila*. Reduction of the dose of the TDMD-regulated miRNAs miR-3 and miR-309 partially rescued embryonic lethality in Dora mutant flies, and loss of the target transcript that triggers TDMD of the miR-310 family impaired cuticle development (Kingston et al. 2022). Thus, in *Drosophila*, regulation of miRNA expression by the TDMD pathway is essential for normal development. Our findings reported here now extend this principle to mammals. Specifically, we demonstrated that reduced dosage of the TDMD-regulated miRNAs miR-322 and miR-503 rescued embryonic growth in ZSWIM8-deficient mice. Loss of a single allele of the *miR-322/503* locus significantly increased body size in *Zswim8*$^{-/-}$ embryos without affecting growth of wild-type embryos, while complete loss of these miRNAs increased body size in all genotypes. These results demonstrate that miR-322 and miR-503 function as dose-dependent regulators of embryonic growth, and the strongly elevated expression of these miRNAs in ZSWIM8-deficient embryos plays a causative role in the growth restriction phenotype. While the specific targets of miR-322 and miR-503 that mediate their growth-sup-

pressive effects remain to be determined, the previously established roles for these miRNAs in regulation of the cell cycle and insulin-like growth factor signaling are promising directions for future investigation, given the central roles of these pathways in mammalian body size regulation (Conlon and Raff 1999; Linsley et al. 2007; Rissland et al. 2011; Llobet-Navas et al. 2014). Further studies in which the dosage of other TDMD-regulated miRNAs is reduced in ZSWIM8-deficient mice or in which TDMD-inducing target sites are ablated will be important to determine whether miRNA dysregulation underlies defective heart and lung development in *Zswim8*$^{-/-}$ embryos.

Looking ahead, a major challenge for the future will be identifying the target sites that trigger decay of the broad set of TDMD-regulated miRNAs described here. Only four endogenous mammalian TDMD triggers have been identified to date (Bitetti et al. 2018; Ghini et al. 2018; Kleaveland et al. 2018; Li et al. 2021), leaving dozens left to be discovered. In order to address this deficit, all modes of target:miRNA interaction that are capable of triggering TDMD must be determined. All known examples of TDMD triggers in mammals exhibit extensive complementarity to both the seed region and 3′ end of the miRNA. Recent work from *C. elegans*, however, has demonstrated that the ZSWIM8 ortholog EBAX-1 can promote the degradation of specific miRNAs in a manner depending only on the seed sequence (Donnelly et al. 2022). This raises the possibility of alternative base-pairing configurations between some miRNAs and their TDMD-inducing targets in mammals. Interestingly, tailing and trimming of miRNAs have been associated with extensive 3′ complementarity to the target, which removes the miRNA 3′ end from the AGO PAZ domain and exposes it to the activity of terminal transferase and exonuclease enzymes (Ameres et al. 2010; Sheu-Gruttadauria et al. 2019; Yang et al. 2020). While many mammalian TDMD substrates exhibit tailing and trimming, some do not, raising the possibility that this latter class of miRNAs may be targeted for TDMD by alternative base-pairing configurations. In these cases, biochemical methods such as cross-linking and immunoprecipitation (CLIP) (Lee and Ule 2018), which could identify RNAs associated with ZSWIM8, might be informative for target identification. Further identification of TDMD triggers and their substrates will be critical for delineating the functions of this important miRNA regulatory pathway in physiology and disease.

Materials and methods

Generation and analysis of genetically engineered mice

All mouse experiments were approved by the University of Texas Southwestern Medical Center Animal Care and Use Committee and performed in accordance with National Institutes of Health guidelines (animal protocol 2017-102001). Mice were group-housed under conventional conditions in a 12-h day/night cycle with ad libitum availability of normal chow diet (Harlan Teklad TD2916) and water. *Nkx2.5*-Cre mice were generously provided

by Dr. Eric Olson and Dr. Rhonda Bassel-Duby (University of Texas Southwestern).

$Zswim8^{-/-}$, $miR322/503^{-/-}$, and $Zswim8^{F/F}$ mice were generated using CRISPR/Cas9-mediated genome editing at the University of Texas Southwestern Transgenic Core. To generate $Zswim8^{-/-}$ and $miR322/503^{-/-}$ mice, Cas9 protein in complex with sgRNAs (Integrated DNA Technologies) were either microinjected or electroporated into the cytoplasm of fertilized C57BL/6J fertilized eggs. To generate $Zswim8^{F/F}$ mice, loxP-containing megamer oligos (Integrated DNA Technologies) were coinjected with Cas9–sgRNA complexes into the pronucleus of fertilized C57BL/6 eggs. Sequences of sgRNAs and megamer are in Supplemental Table S3. Founders carrying the desired alleles were maintained in a pure C57BL/6J background with continuous backcrossing. For timed matings, the morning of detection of vaginal plug was defined as E0.5.

Phenotyping of embryos was performed at E18.5 after delivery by caesarean section. Embryos were weighed and imaged before sacrificing. Tissues were fixed in 10% neutral-buffered formalin (Sigma) overnight, followed by paraffin embedding and sectioning for H&E staining. Tissue sections were imaged using a Zeiss Axio Observer Z1 microscope, and whole-mount images were generated using a Nikon SMZ800N with NIS Elements software (Nikon). High-resolution composite images of the entire section (heart and lungs) were captured using tiling and stitching functions of Zen Pro 3.4 software (Blue edition; Zeiss).

Western blotting

Brains from E18.5 mice were homogenized in lysis buffer (40 mM HEPES at pH 7.4, 2 mM EDTA, 2 mM EGTA, 150 mM NaCl, 1% Triton X-100) supplemented with 1× complete protease inhibitor cocktail and 1× complete phosphatase inhibitor cocktail (Roche) using a Precellys Evolution homogenizer (Bertin Technologies). Approximately 100 µg of lysate was resolved on 8% SDS-PAGE, blotted onto nitrocellulose membranes, and probed with anti-ZSWIM8 (1:400; Thermo PA5-59492) or anti-GAPDH (1:1000; Cell Signaling 2118) followed by HRP-conjugated antirabbit secondary (1:10,000; Jackson ImmunoResearch 111-035-144). Chemiluminescence detection was performed using Femto Clean ECL solution (Thermo Fisher) with a Chemidoc MP imaging station (Bio-Rad).

Quantitative PCR measurement of floxed allele recombination

E18.5 hearts were homogenized using a Precellys Evolution homogenizer (Bertin Technologies), and genomic DNA was extracted using the DNeasy blood and tissue kit (Qiagen). Quantitative PCR was performed with Power SYBR Green PCR master mix (Thermo Fisher) using primers that were specific for the nonrecombined allele. Primers that amplified a region of the $Zswim8$ gene outside of the targeted sequence were used for normalization. Percent recombined was calculated as 1 − (frequency of nonrecombined alleles). Primer sequences are in Supplemental Table S3.

RNA extraction, small RNA sequencing, and Northern blot analysis

Tissues from E18.5 embryos were homogenized in Qiazol (Qiagen) using a Precellys Evolution homogenizer (Bertin Technologies). Total RNA was extracted using the miRNeasy mini RNA isolation kit (Qiagen) and digested with DNase I to remove genomic DNA. Library preparation was performed as previously described (Kim et al. 2019; Han et al. 2020). In brief, total RNA was size-fractionated on a 15% urea–polyacrylamide gel. RNAs were ligated to a 3′ randomized adapter using T4 RNA ligase 2

truncated KQ in buffer supplemented with 20% PEG 8000 overnight at 25°C. Following gel purification, RNAs were ligated to a 5′ randomized adapter using T4 ligase 1 in buffer supplemented with 20% PEG 8000 for 1 h at 37°C. The product was then reverse-transcribed with SuperScript III (Invitrogen), cDNA was PCR-amplified with Phusion polymerase (Thermo Fisher), and the product was gel-purified.

Northern blotting was performed as previously described (Han et al. 2020). In brief, total RNA was run on a 15% urea–polyacrylamide gel and transferred to a nylon membrane before UV crosslinking, blocking, and probing with a radiolabeled probe. A locked nucleic acid probe (mmu-miR-450b-5p miRCURY LNA miRNA fetection probe; Qiagen) was used to detect miR-450b, while standard DNA oligonucleotide probes were used for other miRNAs. Probe sequences are in Supplemental Table S3.

Analysis of small RNA sequencing data

Adapters were trimmed using Cutadapt (Martin 2011), and trimmed reads with low quality (-Q33 -q 20 -p 95) were filtered out using FastX-Toolkit (http://hannonlab.cshl.edu/fastx_toolkit). Reads were assigned to miRNAs in miRbase v22 (Kozomara et al. 2019) based on a perfect match to the first 18 nt of each miRNA. Tailing and trimming were analyzed as previously described (Kleaveland et al. 2018). For each miRNA, the proportion of reads with each observed length was calculated. The minimum length of the normal range (L_{min}) of a miRNA was set as the minimum length with a proportion >14.5%, and the maximum length of the normal range (L_{max}) was set as the maximum length with a proportion >14.5%. The reads with length between L_{min} and L_{max} were defined as nontailed/nontrimmed miRNA, the reads with length less than L_{min} were defined as trimmed miRNA, and reads with length greater than L_{max} were defined as tailed miRNA. EdgeR (Robinson et al. 2010) was used to identify differentially expressed miRNAs between genotypes.

Quantification and statistical analysis

For measurements of body weight, each data point represents a single embryo or mouse. Statistical comparisons were performed using Prism 9. Unpaired t-tests were performed to evaluate differences between genotypes. Unpaired t-tests or Wilcoxon rank sum tests were used to evaluate differences in tailing and trimming between miRNAs. A χ^2 test was used to evaluate the enrichment of clustered miRNAs among TDMD substrates. Significance is indicated as follows: $P < 0.05$ (*), $P < 0.01$ (**), $P < 0.001$ (***), and $P < 0.0001$ (****). All values are reported as mean ± SD.

Data access

Small RNA sequencing data generated in this study have been deposited in GEO (accession no. GSE235065). No custom code was generated in this study.

Competing interest statement

Acknowledgments

References

Ameres SL, Horwich MD, Hung JH, Xu J, Ghildiyal M, Weng ZP, Zamore PD. 2010. Target RNA-directed trimming and tailing of small silencing RNAs. *Science* **328:** 1534–1539. doi:10.1126/science.1187058

Aqeilan RI, Calin GA, Croce CM. 2010. miR-15a and miR-16-1 in cancer: discovery, function and future perspectives. *Cell Death Differ* **17:** 215–220. doi:10.1038/cdd.2009.69

Bail S, Swerdel M, Liu H, Jiao X, Goff LA, Hart RP, Kiledjian M. 2010. Differential regulation of microRNA stability. *RNA* **16:** 1032–1039. doi:10.1261/rna.1851510

Bartel DP. 2018. Metazoan microRNAs. *Cell* **173:** 20–51. doi:10.1016/j.cell.2018.03.006

Bitetti A, Mallory AC, Golini E, Carrieri C, Carreño Gutiérrez H, Pérlas E, Perez-Rico YA, Tocchini-Valentini GP, Enright AJ, Norton WHJ, et al. 2018. MicroRNA degradation by a conserved target RNA regulates animal behavior. *Nat Struct Mol Biol* **25:** 244–251. doi:10.1038/s41594-018-0032-x

Cazalla D, Yario T, Steitz JA. 2010. Down-regulation of a host microRNA by a *Herpesvirus saimiri* noncoding RNA. *Science* **328:** 1563–1566. doi:10.1126/science.1187197

Cheng WC, Chung IF, Huang TS, Chang ST, Sun HJ, Tsai CF, Liang ML, Wong TT, Wang HW. 2013. YM500: a small RNA sequencing (smRNA-seq) database for microRNA research. *Nucleic Acids Res* **41:** D285–D294. doi:10.1093/nar/gks1238

Cloonan N, Wani S, Xu Q, Gu J, Lea K, Heater S, Barbacioru C, Steptoe AL, Martin HC, Nourbakhsh E, et al. 2011. MicroRNAs and their isomiRs function cooperatively to target common biological pathways. *Genome Biol* **12:** R126. doi:10.1186/gb-2011-12-12-r126

Conlon I, Raff M. 1999. Size control in animal development. *Cell* **96:** 235–244. doi:10.1016/s0092-8674(00)80563-2

Donnelly BF, Yang B, Grimme AL, Vieux KF, Liu CY, Zhou L, McJunkin K. 2022. The developmentally timed decay of an essential microRNA family is seed-sequence dependent. *Cell Rep* **40:** 111154. doi:10.1016/j.celrep.2022.111154

Elkayam E, Kuhn CD, Tocilj A, Haase AD, Greene EM, Hannon GJ, Joshua-Tor L. 2012. The structure of human argonaute-2 in complex with miR-20a. *Cell* **150:** 100–110. doi:10.1016/j.cell.2012.05.017

Gantier MP, McCoy CE, Rusinova I, Saulep D, Wang D, Xu D, Irving AT, Behlke MA, Hertzog PJ, Mackay F, et al. 2011. Analysis of microRNA turnover in mammalian cells following Dicer1 ablation. *Nucleic Acids Res* **39:** 5692–5703. doi:10.1093/nar/gkr148

Gatfield D, Le Martelot G, Vejnar CE, Gerlach D, Schaad O, Fleury-Olela F, Ruskeepää AL, Oresic M, Esau CC, Zdobnov EM, et al. 2009. Integration of microRNA miR-122 in hepatic circadian gene expression. *Genes Dev* **23:** 1313–1326. doi:10.1101/gad.1781009

Gebert LFR, MacRae IJ. 2019. Regulation of microRNA function in animals. *Nat Rev Mol Cell Biol* **20:** 21–37. doi:10.1038/s41580-018-0045-7

Ghini F, Rubolino C, Climent M, Simeone I, Marzi MJ, Nicassio F. 2018. Endogenous transcripts control miRNA levels and activity in mammalian cells by target-directed miRNA degradation. *Nat Commun* **9:** 3119. doi:10.1038/s41467-018-05182-9

Griffiths-Jones S, Hui JH, Marco A, Ronshaugen M. 2011. MicroRNA evolution by arm switching. *EMBO Rep* **12:** 172–177. doi:10.1038/embor.2010.191

Grimson A, Srivastava M, Fahey B, Woodcroft BJ, Chiang HR, King N, Degnan BM, Rokhsar DS, Bartel DP. 2008. Early origins and evolution of microRNAs and Piwi-interacting RNAs in animals. *Nature* **455:** 1193–1197. doi:10.1038/nature07415

Guo Y, Liu J, Elfenbein SJ, Ma Y, Zhong M, Qiu C, Ding Y, Lu J. 2015. Characterization of the mammalian miRNA turnover landscape. *Nucleic Acids Res* **43:** 2326–2341. doi:10.1093/nar/gkv057

Han J, LaVigne CA, Jones BT, Zhang H, Gillett F, Mendell JT. 2020. A ubiquitin ligase mediates target-directed microRNA decay independently of tailing and trimming. *Science* **370:** eabc9546. doi:10.1126/science.abc9546

Hwang HW, Wentzel EA, Mendell JT. 2007. A hexanucleotide element directs microRNA nuclear import. *Science* **315:** 97–100. doi:10.1126/science.1136235

Jeong HC, Shukla S, Fok WC, Huynh TN, Batista LFZ, Parker R. 2023. USB1 is a miRNA deadenylase that regulates hematopoietic development. *Science* **379:** 901–907. doi:10.1126/science.abj8379

Jonas S, Izaurralde E. 2015. Towards a molecular understanding of microRNA-mediated gene silencing. *Nat Rev Genet* **16:** 421–433. doi:10.1038/nrg3965

Kabekkodu SP, Shukla V, Varghese VK, D'Souza J, Chakrabarty S, Satyamoorthy K. 2018. Clustered miRNAs and their role in biological functions and diseases. *Biol Rev Camb Philos Soc* **93:** 1955–1986. doi:10.1111/brv.12428

Kim VN, Han J, Siomi MC. 2009. Biogenesis of small RNAs in animals. *Nat Rev Mol Cell Biol* **10:** 126–139. doi:10.1038/nrm2632

Kim H, Kim J, Kim K, Chang H, You K, Kim VN. 2019. Bias-minimized quantification of microRNA reveals widespread alternative processing and 3′ end modification. *Nucleic Acids Res* **47:** 2630–2640. doi:10.1093/nar/gky1293

Kingston ER, Bartel DP. 2019. Global analyses of the dynamics of mammalian microRNA metabolism. *Genome Res* **29:** 1777–1790. doi:10.1101/gr.251421.119

Kingston ER, Blodgett LW, Bartel DP. 2022. Endogenous transcripts direct microRNA degradation in *Drosophila*, and this targeted degradation is required for proper embryonic development. *Mol Cell* **82:** 3872–3884.e9. doi:10.1016/j.molcel.2022.08.029

Kleaveland B, Shi CY, Stefano J, Bartel DP. 2018. A network of noncoding regulatory RNAs acts in the mammalian brain. *Cell* **174:** 350–362.e17. doi:10.1016/j.cell.2018.05.022

Kozomara A, Birgaoanu M, Griffiths-Jones S. 2019. miRBase: from microRNA sequences to function. *Nucleic Acids Res* **47:** D155–D162. doi:10.1093/nar/gky1141

Krol J, Busskamp V, Markiewicz I, Stadler MB, Ribi S, Richter J, Duebel J, Bicker S, Fehling HJ, Schübeler D, et al. 2010. Characterizing light-regulated retinal microRNAs reveals rapid turnover as a common property of neuronal microRNAs. *Cell* **141:** 618–631. doi:10.1016/j.cell.2010.03.039

Lee FCY, Ule J. 2018. Advances in CLIP technologies for studies of protein-RNA interactions. *Mol Cell* **69:** 354–369. doi:10.1016/j.molcel.2018.01.005

Lee S, Song J, Kim S, Kim J, Hong Y, Kim Y, Kim D, Baek D, Ahn K. 2013. Selective degradation of host microRNAs by an intergenic HCMV noncoding RNA accelerates virus production. *Cell Host Microbe* **13:** 678–690. doi:10.1016/j.chom.2013.05.007

Li SC, Liao YL, Chan WC, Ho MR, Tsai KW, Hu LY, Lai CH, Hsu CN, Lin WC. 2011. Interrogation of rabbit miRNAs and their isomiRs. *Genomics* **98:** 453–459. doi:10.1016/j.ygeno.2011.08.008

Li SC, Liao YL, Ho MR, Tsai KW, Lai CH, Lin WC. 2012. miRNA arm selection and isomiR distribution in gastric cancer. *BMC Genomics* **13 Suppl 1:** S13. doi:10.1186/1471-2164-13-S1-S13

Li L, Sheng P, Li T, Fields CJ, Hiers NM, Wang Y, Li J, Guardia CM, Licht JD, Xie M. 2021. Widespread microRNA degradation elements in target mRNAs can assist the encoded proteins. *Genes Dev* **35:** 1595–1609. doi:10.1101/gad.348874.121

Libri V, Helwak A, Miesen P, Santhakumar D, Borger JG, Kudla G, Grey F, Tollervey D, Buck AH. 2012. Murine cytomegalovirus encodes a miR-27 inhibitor disguised as a target. *Proc Natl Acad Sci* **109:** 279–284. doi:10.1073/pnas.1114204109

Linsley PS, Schelter J, Burchard J, Kibukawa M, Martin MM, Bartz SR, Johnson JM, Cummins JM, Raymond CK, Dai H, et al. 2007. Transcripts targeted by the microRNA-16 family cooperatively regulate cell cycle progression. *Mol Cell Biol* **27:** 2240–2252. doi:10.1128/MCB.02005-06

Llobet-Navas D, Rodríguez-Barrueco R, Castro V, Ugalde AP, Sumazin P, Jacob-Sendler D, Demircan B, Castillo-Martín M, Putcha P, Marshall N, et al. 2014. The *miR-424(322)/503* cluster orchestrates remodeling of the epithelium in the involuting mammary gland. *Genes Dev* **28:** 765–782. doi:10.1101/gad.237404.114

Marcinowski L, Tanguy M, Krmpotic A, Rädle B, Lisnić VJ, Tuddenham L, Chane-Woon-Ming B, Ruzsics Z, Erhard F, Benkartek C, et al. 2012. Degradation of cellular mir-27 by a novel, highly abundant viral transcript is important for efficient virus replication in vivo. *PLoS Pathog* **8:** e1002510. doi:10.1371/journal.ppat.1002510

Marco A, Hui JH, Ronshaugen M, Griffiths-Jones S. 2010. Functional shifts in insect microRNA evolution. *Genome Biol Evol* **2:** 686–696. doi:10.1093/gbe/evq053

Martin M. 2011. Cutadapt removes adapter sequences from high-throughput sequencing reads. *EMBnetj* **17:** 10–12. doi:10.14806/ej.17.1.200

Marzi MJ, Ghini F, Cerruti B, de Pretis S, Bonetti P, Giacomelli C, Gorski MM, Kress T, Pelizzola M, Muller H, et al. 2016. Degradation dynamics of microRNAs revealed by a novel pulse-chase approach. *Genome Res* **26:** 554–565. doi:10.1101/gr.198788.115

McFadden DG, Barbosa AC, Richardson JA, Schneider MD, Srivastava D, Olson EN. 2005. The Hand1 and Hand2 transcription factors regulate expansion of the embryonic cardiac ventricles in a gene dosage-dependent manner. *Development* **132:** 189–201. doi:10.1242/dev.01562

Medley JC, Panzade G, Zinovyeva AY. 2021. MicroRNA strand selection: unwinding the rules. *Wiley Interdiscip Rev RNA* **12:** e1627. doi:10.1002/wrna.1627

Reichholf B, Herzog VA, Fasching N, Manzenreither RA, Sowemimo I, Ameres SL. 2019. Time-resolved small RNA sequencing unravels the molecular principles of microRNA homeostasis. *Mol Cell* **75:** 756–768.e7. doi:10.1016/j.molcel.2019.06.018

Rissland OS, Hong SJ, Bartel DP. 2011. MicroRNA destabilization enables dynamic regulation of the miR-16 family in response to cell-cycle changes. *Mol Cell* **43:** 993–1004. doi:10.1016/j.molcel.2011.08.021

Robinson MD, McCarthy DJ, Smyth GK. 2010. Edger: a Bioconductor package for differential expression analysis of digital gene expression data. *Bioinformatics* **26:** 139–140. doi:10.1093/bioinformatics/btp616

Schirle NT, MacRae IJ. 2012. The crystal structure of human Argonaute2. *Science* **336:** 1037–1040. doi:10.1126/science.1221551

Sheng P, Li L, Li T, Wang Y, Hiers NM, Mejia JS, Sanchez JS, Zhou L, Xie M. 2023. Screening of *Drosophila* microRNA-degradation sequences reveals Argonaute1 mRNA's role in regulating miR-999. *Nat Commun* **14:** 2108. doi:10.1038/s41467-023-37819-9

Sheu-Gruttadauria J, Pawlica P, Klum SM, Wang S, Yario TA, Schirle Oakdale NT, Steitz JA, MacRae IJ. 2019. Structural basis for target-directed microRNA degradation. *Mol Cell* **75:** 1243–1255.e7. doi:10.1016/j.molcel.2019.06.019

Shi CY, Kingston ER, Kleaveland B, Lin DH, Stubna MW, Bartel DP. 2020. The ZSWIM8 ubiquitin ligase mediates target-directed microRNA degradation. *Science* **370:** eabc9359. doi:10.1126/science.abc9359

Shukla S, Bjerke GA, Muhlrad D, Yi R, Parker R. 2019. The RNase PARN controls the levels of specific miRNAs that contribute to p53 regulation. *Mol Cell* **73:** 1204–1216.e4. doi:10.1016/j.molcel.2019.01.010

Turgeon B, Meloche S. 2009. Interpreting neonatal lethal phenotypes in mouse mutants: insights into gene function and human diseases. *Physiol Rev* **89:** 1–26. doi:10.1152/physrev.00040.2007

van Rooij E, Sutherland LB, Qi X, Richardson JA, Hill J, Olson EN. 2007. Control of stress-dependent cardiac growth and gene expression by a microRNA. *Science* **316:** 575–579. doi:10.1126/science.1139089

Vidigal JA, Ventura A. 2015. The biological functions of miRNAs: lessons from in vivo studies. *Trends Cell Biol* **25:** 137–147. doi:10.1016/j.tcb.2014.11.004

Wang Z, Hou Y, Guo X, van der Voet M, Boxem M, Dixon JE, Chisholm AD, Jin Y. 2013. The EBAX-type cullin-RING E3 ligase and Hsp90 guard the protein quality of the SAX-3/Robo receptor in developing neurons. *Neuron* **79:** 903–916. doi:10.1016/j.neuron.2013.06.035

Wang G, Lei J, Wang Y, Yu J, He Y, Zhao W, Hu Z, Xu Z, Jin Y, Gu Y, et al. 2023. The ZSWIM8 ubiquitin ligase regulates neurodevelopment by guarding the protein quality of intrinsically disordered Dab1. *Cereb Cortex* **33:** 3866–3881. doi:10.1093/cercor/bhac313

Warburton D, El-Hashash A, Carraro G, Tiozzo C, Sala F, Rogers O, De Langhe S, Kemp PJ, Riccardi D, Torday J, et al. 2010. Lung organogenesis. *Curr Top Dev Biol* **90:** 73–158. doi:10.1016/S0070-2153(10)90003-3

Yang A, Shao TJ, Bofill-De Ros X, Lian C, Villanueva P, Dai L, Gu S. 2020. AGO-bound mature miRNAs are oligouridylated by TUTs and subsequently degraded by DIS3L2. *Nat Commun* **11:** 2765. doi:10.1038/s41467-020-16533-w